ISSN 0021-3640, JETP Letters, 2024, Vol. 119, No. 3, pp. 233–250. © Pleiades Publishing, Ltd., 2024.
ISSN 0021-3640, JETP Letters, 2024. © Pleiades Publishing, Ltd., 2024.
Russian Text © The Author(s), 2024, published in Pis'ma v Zhurnal Eksperimental'noi i Teoreticheskoi Fiziki, 2024, Vol. 119, No. 3, pp. 234–252.

CONDENSED MATTER

Suppression of Superconducting Fluctuations in Multiband Superconductors as a Mechanism for Increasing the Critical Temperature (Brief Review)

A. V. Krasavin[a,b,*], A. V. Vagov[b], A. S. Vasenko[b,c], V. A. Stolyarov[d,e,f], and A. A. Shanenko[b]

[a] *National Research Nuclear University MEPhI, Moscow, 115409 Russia*
[b] *National Research University Higher School of Economics, Moscow, 101000 Russia*
[c] *Tamm Department of Theoretical Physics, Lebedev Physical Institute, Russian Academy of Sciences, Moscow, 119991 Russia*
[d] *National University of Science and Technology MISIS, Moscow, 119049 Russia*
[e] *Centre for Advanced Mesoscience and Nanotechnology, Moscow Institute of Physics and Technology, Dolgoprudny, Moscow region, 141700 Russia*
[f] *Dukhov Automatics Research Institute, Moscow, 127055 Russia*
**e-mail: avkrasavin@gmail.com*

Received November 22, 2023; revised December 4, 2023; accepted December 7, 2023

The combination of strongly coupled Cooper pairs and weak superconducting fluctuations is an important prerequisite for achieving high-temperature superconductivity. The review is devoted to the implementation of this condition in multiband superconductors, in which strongly coupled pairs in the shallow conduction band (the Fermi level is close to the band edge) coexist with ordinary, weakly fluctuating Cooper pairs formed in the deep band. As a result of the Josephson coupling between condensates in different bands, such a system is characterized by a high critical coherence temperature due to the presence of strongly coupled pairs and the suppression of superconducting fluctuations. This suppression does not require any special preconditions, and is almost total even if the Josephson coupling between the bands is weak.

DOI: 10.1134/S0021364023603755

1. INTRODUCTION

1.1. Multiband Superconductors

Explaining the phenomenon of superconductivity and exploring the possibilities for its use are among the main goals of modern condensed matter physics. Despite the fact that at the moment there is no complete universal theory of superconductivity applicable to any materials, solid state physics has made significant progress in understanding the properties and technological applications of traditional superconductors, which include metals and alloys that become superconducting at very low temperatures (below 30 K).

Superconductors that do not fall into this category are often called unconventional. They tend to have a more complex crystal structure and may have pairing mechanisms that differ from the standard Bardeen–Cooper–Schrieffer (BCS) [1] theory of superconductivity. Compared to superconductors described by the BCS theory, such materials often have higher critical temperature, which makes it possible practical applications under more accessible cooling conditions. One of the common materials of this type are cuprate superconductors [2], based on copper oxide compounds. Cuprate superconductors have critical temperatures reaching up to 133 K at normal pressure. However, the mechanisms of superconductivity in these materials are not fully understood, which makes their study an area of active research [3–7].

The band structure of many of these compounds has a similar configuration [8], shown schematically in Fig. 1. Their distinctive feature is the presence of a shallow band for which the Fermi level is close to the band edge. Such a band structure is characteristic of the vicinity of the Lifshitz phase transition, in which the topology of the Fermi surface changes [9, 10]. Here we show that this configuration of the band structure can lead to a significant increase in the critical temperature of the superconducting transition. This possibility is achieved due to the interaction of strongly coupled charge carrier pairs formed in the shallow band with ordinary Cooper pairs existing in other, deep bands of the superconductor.

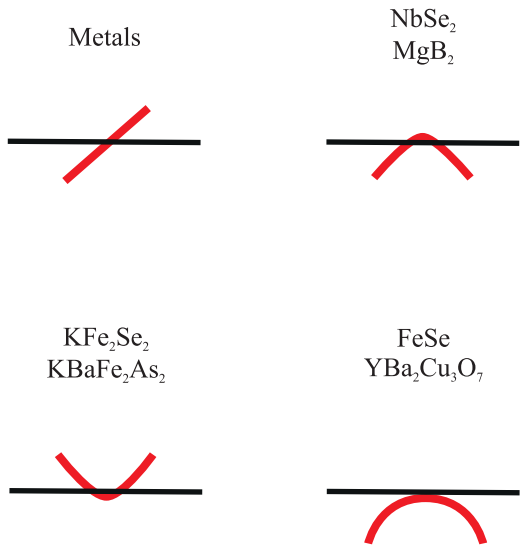

Fig. 1. (Color online) Schematic representation of the band structure of some superconducting compounds in comparison with the band structure of metals. Key: 1. Metals

This mechanism is applicable to many compounds where the multiband or multigap superconductivity takes place, and the amplitudes of the superconducting gaps corresponding to different sheets of the Fermi surface vary considerably. This may occur, for example, due to different band dimensions, as in the case of MgB_2, due to the presence of repulsive interband pair interactions, as in the case of most iron-based superconductors, or due to the appearance of multiple pockets on the Fermi surface due to crystal symmetry, as in $FeSe_xTe_{1-x}$ [11]. In such compounds, interband pairing is usually suppressed due to the large difference in wave functions of charge carriers in different bands. Therefore, with good accuracy, band condensates are formed by Cooper pairing of carriers in each of the bands separately.

In multiband systems, a larger number of degrees of freedom of the condensate wave function gives rise to quantum effects that cannot occur in single-band superconductors. The key characteristic is the possibility of interference between the band condensates. The interference results in screening fluctuations of the superconducting order parameter. This opens a direct path to an increase in the critical temperature.

1.2. Mean Field Theory and Fluctuations

For many decades, the BCS theory has been a powerful tool for studying superconductivity. Being essentially a mean field theory, the BCS approach is particularly successful in describing the superconducting transition in traditional superconductors. In these materials, fluctuations of the superconducting order parameter do not play a significant role in almost the entire temperature range; the critical region, where they are significant, is very narrow [12, 13] and practically unattainable for experiment. On the contrary, in many superconducting materials with a high critical temperature (high-temperature superconductors or HTSC), this region can expand greatly.

Superconducting fluctuations are random changes in the wave function of the condensate (superconducting order parameter), which determines the macroscopic properties of the superconducting state. In traditional materials that can be described by the BCS theory, such fluctuations are insignificant, so that random deviations of the order parameter below the critical temperature are practically negligible, which corresponds to ideal superconductivity. However, in high-temperature superconductors, fluctuations remain pronounced well below the critical temperature, leading to a significant deviation from superconducting behavior, resulting in the appearance of nonzero resistivity. For such compounds, the question of the influence of fluctuations on the critical transition temperature becomes relevant, as the latter may be substantially decreased due to strong fluctuations.

Indeed, fluctuations of the superconducting order parameter are one of the main factors suppressing superconductivity at temperatures below the critical mean field temperature T_{c0}. Although Cooper pairs are formed at temperatures $T < T_{c0}$, the transition to the superconducting state occurs at a lower critical temperature $T_c < T_{c0}$. In the interval $T_c < T < T_{c0}$ the system is in the so-called pseudogap state [3, 5, 7] characterized by the absence of coherence of preformed Cooper pairs. The role of fluctuations increases with the decreasing dimensionality of the system, so that for quasi-one-dimensional materials one has $T_c \ll T_{c0}$ (see, e.g., [14–16]).

The shift in the critical temperature due to fluctuations, however, is not a universal property of all superconducting materials. Thus, studying the mechanisms of the influence of fluctuations on the superconducting state and developing strategies to control them, is of utmost importance when one wants to achieve the higher critical temperature.

The mechanism for increasing the critical temperature discussed in this review is based on the interaction of two bands in a multiband superconductor. The system is assumed to be close to the Lifshitz transition because one of the bands is shallow. The superconducting condensate in this band finds itself between the regimes of weakly coupled Cooper pairs (BSC) and of strongly coupled molecules (Bose–Einstein condensate or BEC), referred to as BCS–BEC crossover [17–24]. It is characterized by a high mean-field critical temperature and large fluctuations. The second band in this system is assumed deep, being in the usual BCS regime of weakly coupled Cooper pairs; it is characterized by a low critical temperature and weak superconducting fluctuations. It turns out that

the interaction between the bands suppresses strong fluctuations in the shallow band, but the critical temperature of the entire system remains close to the mean field critical temperature T_{c0} of the shallow band.

The multiband mechanism for the fluctuation suppression is considered in this review in relation to superconductors with ordinary *s*-wave pairing, as in the standard BCS theory. However, a similar effect is expected in systems with *d*-type pairing. In addition, we limit ourselves to the study of a two-band system, which is considered as a prototype of a multi-band superconductor. The entire formalism is easily generalized to the case of a larger number of conduction bands, and the qualitative conclusions remain the same.

2. FLUCTUATIONS IN A TWO-BAND SUPERCONDUCTOR

2.1. Microscopic Description of the System

The analysis of a two-band (in general, multiband) superconductor with conventional *s*-symmetry pairing in each band employs a standard generalization of the BCS model to the situation with several types of charge carriers. We recall that, within the framework of this generalization, Cooper pairing is described by the interaction

$$V_{BCS} = -\sum_{\nu,\nu'} g_{\nu\nu'} \int d\mathbf{r} \psi^{\dagger}_{\nu\uparrow} \psi^{\dagger}_{\nu\downarrow} \psi_{\nu'\downarrow} \psi_{\nu'\uparrow}, \qquad (1)$$

where $\psi^{\dagger}_{\nu\sigma} \equiv \psi^{\dagger}_{\nu\sigma}(\mathbf{r})$ and $\psi_{\nu\sigma} \equiv \psi_{nu\sigma}(\mathbf{r})$ are charge carrier operators in the band ν ($\nu = 1, 2$); g is the scattering matrix, $g_{\nu\nu'} = g_{\nu'\nu}$, and the expression (1) is obtained under the standard assumption that the elements of the matrix g depend weakly on momentum and this dependence can be neglected.

In the mean field approximation and in the absence of impurities (in the so-called "pure limit") and interband pairing, the Hamiltonian of the superconducting system may be written in the form [25, 26]

$$H = \sum_{\nu} \int d\mathbf{r} [\psi^{\dagger}_{\nu\sigma} T_{\nu}(\mathbf{r}) \psi_{\nu\sigma} + (\psi^{\dagger}_{\nu\uparrow} \psi^{\dagger}_{\nu\downarrow} \Delta_{\nu}(\mathbf{r}) + \text{H.c.})] + (\mathbf{\Delta}, g^{-1}\mathbf{\Delta}), \qquad (2)$$

where $T_{\nu}(\mathbf{r})$ is the single-particle energy operator, and the gap functions for a two-band system are written as a vector $\mathbf{\Delta} \equiv (\Delta_1, \Delta_2)^T$ with the scalar product $(A, B) \equiv \sum_{\nu} A^*_{\nu} B_{\nu}$, so that the last term in the equation (2) is written explicitly in the form

$$(\mathbf{\Delta}, g^{-1}\mathbf{\Delta}) = \frac{1}{G} \int d\mathbf{r} [g_{22}|\Delta_1|^2 + g_{11}|\Delta_2|^2 + g_{12}(\Delta^*_1 \Delta_2 + \Delta^*_2 \Delta_1)], \qquad (3)$$

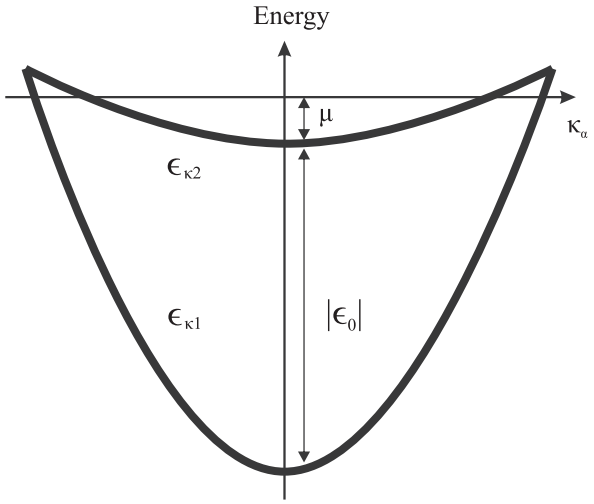

Fig. 2. Schematic representation of the band structure. The deep band $\nu = 1$ is three-dimensional or quasi-two-dimensional, the band $\nu = 2$ is shallow and low-dimensional. The corresponding dispersion relations reads as

$$\epsilon_{\mathbf{k}1} = \epsilon_0 + \sum_{\alpha} \frac{\hbar^2 k_{\alpha}^2}{2m_1} - \mu, \; \epsilon_{\mathbf{k}2} = \sum_{\beta} \frac{\hbar^2 k_{\beta}^2}{2m_2} - \mu; \; |\mu| \ll |\epsilon_0|.$$

where $G = g_{11}g_{22} - g_{12}^2$. In Equations ((2)) and ((3)), the gap functions satisfy the mean field self-consistency equation

$$\Delta_{\nu} = \sum_{\nu'} g_{\nu\nu'} \langle \psi_{\nu'\uparrow} \psi_{\nu'\downarrow} \rangle, \qquad (4)$$

where $\langle \ldots \rangle$ denotes anomalous averages related to the corresponding Green's functions. The absence of interband Cooper pairing is reflected in the fact that this expression contains only operators with the same band indices ν.

In this review, we consider special configurations of the band structure of a two-band superconductor, a schematic representation of which is shown in Fig. 2. One of the bands, say $\nu = 1$, is three-dimensional (3D) or quasi-two-dimensional (Q2D) and "deep", i.e., its minimum (band bottom or edge) is located far from the Fermi level, $|\epsilon_0| \ll \mu$. The second band ($\nu = 2$) is quasi-one-dimensional (Q1D) or quasi-two-dimensional (Q2D) and "shallow", i.e., the Fermi level is located relatively close to its edge. In such a system, the superconducting condensate is a coherent mixture of a BCS condensate in the deep band and a condensate in the BCS–BEC crossover regime in the shallow band. In the BCS–BEC crossover, the size of the Cooper pair is comparable to the average distance between particles, $\xi \sim 1/k_F$, where k_F is the Fermi momentum. Equivalently, the characteristic pairing energy is of the order of the Fermi energy, $\Delta \sim E_F$. The BCS and BEC states correspond to inequalities $k_F\xi \gg 1$ and $k_F\xi \ll 1$, respectively. The BCS–BEC crossover was first observed experimentally in a system

of ultracold Fermi gases (see, for example, [27]), for which the interparticle interaction is controlled using the Feshbach resonance [28]. In solid-state systems, tuning the crossover is a much more complex task that involves changing the ratio Δ/E_F by using chemical engineering, doping, changing the substrate material, or varying other system attributes.

2.2. Free Energy Functional

To calculate fluctuation corrections, it is necessary to obtain the free energy of the system in the form of a functional of the gap functions Δ_ν. The contribution of fluctuations is then taken into account by averaging the relevant physical quantities over random variations of the gap functions Δ_ν with the statistical Gibbs weight for the free energy. Within the microscopic BCS theory, these calculations are too complex for practical use. In the case of one band, the analysis is usually limited to the most important contribution in the free energy expansion, described by the Ginzburg–Landau (GL) functional [29]. This approach is thoroughly justified, especially near the critical transition temperature T_{c0}.

For a two-band superconductor, the same expansion can be made, while keeping in each band only those contributions that correspond to the standard GL theory. Near the critical temperature T_{c0}, the corresponding energy functional is obtained by expanding the thermodynamic potential with respect to small gap functions Δ_ν, derived using the microscopic Hamiltonian (2). Obtaining this decomposition for each band of the two-band model is completely equivalent to the one-band case [29]. The calculation gives the following expression for free energy (see, for example, [30–32]):

$$F = \int d\mathbf{r}\left[\sum_\nu f_\nu + (\mathbf{\Delta}, \mathscr{L}\mathbf{\Delta})\right],$$

$$f_\nu = a_\nu|\Delta_\nu|^2 + \frac{b_\nu}{2}|\Delta_\nu|^4 + \sum_i \mathscr{K}_\nu^{(i)}|\nabla_i\Delta_\nu|^2,$$

$$\mathscr{L} = g^{-1} - \begin{bmatrix} \mathscr{A}_1 & 0 \\ 0 & \mathscr{A}_2 \end{bmatrix}. \quad (5)$$

Coefficients a_ν, b_ν, $\mathscr{K}_\nu^{(i)}$, and $\mathscr{A}_\nu$ in this expression depend on the dimensionality of the corresponding band and its microscopic parameters, the index i marks spatial coordinate axis of the band, and the magnetic field is set assumed zero. The field-related corrections for the temperature fluctuations is discussed at the end of the section.

2.3. Efficient One-component Free Energy Functional

To use functional F in Eq. (5) in the calculations we first separate out the largest contribution to the fluctuations near the critical temperature T_{c0}. To do this, we recall that within the mean field approximation T_{c0} is determined from the solution of the linearized gap (self-consistency) Eq. (4), which reads

$$\mathscr{L}\mathbf{\Delta} = 0. \quad (6)$$

This equation has a nontrivial solution under the condition

$$\det[\mathscr{L}] = 0, \quad (7)$$

from which the mean field critical temperature T_{c0} is found. In the case of two bands, this equation has two solutions from which one has to take the largest T_{c0}, as this solution corresponds to the minimal free energy. The gap function corresponding to this solution satisfies the relation

$$\mathbf{\Delta}(\mathbf{r}) = \boldsymbol{\eta}_+\psi(\mathbf{r}), \quad \boldsymbol{\eta}_+ = \begin{pmatrix} 1 \\ S \end{pmatrix}, \quad (8)$$

where $\psi(\mathbf{r})$ is an arbitrary function of coordinates and S is defined as

$$S = \frac{g_{22} - G\mathscr{A}_1}{g_{12}}. \quad (9)$$

Clearly, Eq. (8) is not the only choice of the eigenvector $\boldsymbol{\eta}_+$ corresponding to the zero eigenvalue of matrix $\mathscr{L}$ since the normalization does not matter.

If we now choose a vector orthogonal to $\boldsymbol{\eta}_+$ in the form

$$\boldsymbol{\eta}_- = \begin{pmatrix} -S \\ 1 \end{pmatrix}, \quad (10)$$

then an arbitrary order parameter vector function can be represented as a sum [33, 34]

$$\mathbf{\Delta}(\mathbf{r}) = \psi(\mathbf{r})\boldsymbol{\eta}_+ + \phi(\mathbf{r})\boldsymbol{\eta}_-, \quad (11)$$

where $\psi(\mathbf{r})$ and $\phi(\mathbf{r})$ describe two different fluctuation modes corresponding to these vectors.

In terms of ψ and ϕ, the free energy F in Eq. (5) is split into the following three contributions,

$$F = \int d\mathbf{r}(f_\psi + f_\phi + f_{\psi\phi}), \quad (12)$$

where the first two give independent contributions of each of the two modes, and the third is the energy of their interaction.

The first contribution f_ψ has the form of a standard GL functional [29, 35]

$$f_\psi = a_\psi|\psi|^2 + \frac{b_\psi}{2}|\psi|^4 + \sum_i \mathscr{K}_\psi^{(i)}|\nabla_i\psi|^2, \quad (13)$$

where the coefficients are given by averaging over the band contributions [33, 34, 36, 37]

$$a_\psi = \sum_\nu \eta_{+,\nu}^2 a_\nu, \quad b_\psi = \sum_\nu \eta_{+,\nu}^4 b_\nu,$$

$$\mathcal{K}_{\psi}^{(i)} = \sum_{\nu} \eta_{+,\nu}^{2} \mathcal{K}_{\nu}^{(i)}. \quad (14)$$

Contribution f_ϕ in Eq. (12) also has the form of Eq. (13), where $\psi(\mathbf{r})$ changes to $\phi(\mathbf{r})$, and the corresponding coefficients are given by [33, 34, 36, 37]

$$a_\phi = a_\phi^{(0)} + \sum_{\nu} \eta_{-,\nu}^{2} a_\nu, \quad b_\phi = \sum_{\nu} \eta_{-,\nu}^{4} b_\nu,$$
$$\mathcal{K}_{\phi}^{(i)} = \sum_{\nu} \eta_{-,\nu}^{2} \mathcal{K}_{\nu}^{(i)}, \quad (15)$$

where $a_\phi^{(0)}$ takes the form

$$a_\phi^{(0)} = (\boldsymbol{\eta}_-, \mathcal{L}\boldsymbol{\eta}_-) = \frac{g_{12}(1+S^2)^2}{GS}. \quad (16)$$

The functional $f_{\psi\phi}$ in (12) describes the interaction of two modes.

The contributions of f_ϕ and $f_{\psi\phi}$ can be neglected since the mode ϕ is not critical. This follows from that $a_\phi^{(0)} \neq 0$ in Equation (15). From Eq. (9) it follows that S is a real quantity, and, therefore, the constant $a_\phi^{(0)}$ is generally non-zero at $T \to T_{c0}$. This implies that the characteristic length $\xi_\phi^{(i)} = \sqrt{\mathcal{K}_\phi^{(i)}/a_\phi}$ of the mode ϕ is not critical (divergent) near T_{c0}. Consequently, the only mode responsible for the critical behavior of the system is ψ with a divergent characteristic length $\xi_\psi^{(i)} = \sqrt{\mathcal{K}_{psi}^{(i)}/a_\psi}$, since the coefficient $a_\psi \to 0$ at $T \to T_{c0}$. The ϕ mode introduces insignificant corrections that can be neglected near T_{c0}.

The fluctuation part of F can thus be approximated using a single mode ψ, with the energy functional given by Eq. (13). The fact that there are two interacting bands in the system is reflected in their contributions to the coefficients a_ψ, b_ψ and $\mathcal{K}_\psi^{(i)}$ in Eq. (14). Therefore, Eq. (13) defines the effective GL theory for a two-band system. Note that it has a single order parameter ψ in full accordance with the Landau theory of phase transitions in the equilibrium system under consideration (see discussion in [38–41]). Fluctuations of this order parameter are critical and dominate in the system when it is near the phase transition. Non-critical fluctuations in the mode ϕ induce some changes in the coefficients of the functional f_ψ, but these are insignificant due to the non-critical nature of the mode and can, therefore, be neglected.

3. FLUCTUATION SHIFT OF CRITICAL TEMPERATURE

3.1. General Remarks

The value of T_{c0} obtained by solving the linearized gap Eq. (6) gives the critical temperature within the mean field approximation. The real superconducting transition temperature T_c will always be lower than T_{c0} due to thermal fluctuations, i.e. the system exhibits a fluctuation-induced shift in the critical temperature. This can be estimated by taking advantage of the fact that the effective free energy functional (13) of the system has a one-component order parameter, which makes it possible to use the results for fluctuation corrections for the conventional one-component GL theory. However, it should be remembered that the same component ψ describes fluctuations of the order parameter in both bands, $\delta\Delta_1 = \delta\psi$, $\delta\Delta_2 = S\delta\psi$, and, therefore, $\delta\Delta_1$ and $\delta\Delta_2$ are not independent. Due to this, some qualitative conclusions can be easily drawn from the very form of the functional and its coefficients in Eq. (14).

For example, if the weight factor is very small, $S \ll 1$, then the gap of the second band $\Delta_2 \to S\psi$ makes virtually no contribution to the free energy F, and the superconducting properties are completely determined by the first band, $\nu = 1$. In the case, where the weight factor $S \gg 1$, the opposite limit is realized, and the contribution of the band $\nu = 2$ is decisive. Crossover between these two limiting cases occurs over a range of values of $S \sim 1$, where the contribution of one band is gradually replaced by that of the other. However, it is important that the coefficients of the energy functional given in Eq. (14), depend on S in different ways leading to different dependencies of the physical characteristics of the system on S. As a consequence, the crossover interval between two limiting regimes depends on what physical quantity we consider.

In particular, fluctuations and critical temperature have different dependencies on system parameters. This is the main reason why it is possible to simultaneously obtain a strong increase in the critical temperature, which is determined by the influence of one (shallow) band, and a suppression of fluctuations, which occurs due to the predominant influence of another (deep) band. The main question is whether it is possible to find an interval of the system parameters in which the decrease in the critical temperature T_c due to fluctuations compared to the mean field value T_{c0} is not too significant, while the mean field temperature has not yet decreased because the deep band becomes dominant. It can be shown that this situation is indeed observed in a wide range of parameters and for many configurations where one band is shallow.

The influence of thermal fluctuations on the critical temperature of the superconducting transition can be roughly estimated from the Ginzburg–Levanyuk parameter (also known as the Ginzburg number)

$$\mathrm{Gi} = 1 - \frac{T_{\mathrm{Gi}}}{T_{c0}}, \quad (17)$$

where T_{Gi} is the temperature at which the fluctuations contribution to the heat capacity becomes equal to the heat capacity calculated using the mean field approximation. Physically, this means that in the temperature range $T_{\mathrm{Gi}} < T < T_{c0}$ the influence of fluctuations is significant.

The Ginzburg number is found by calculating the heat capacity using the energy functional (13). A qualitative estimate [42] gives the following result

$$\mathrm{Gi} \propto \left(\frac{T_{c0}}{E_F}\right)^{\frac{2(D-1)}{4-D}}, \qquad (18)$$

where E_F is the Fermi energy, and D is the system dimensionality. More accurate calculations for the isotropic case for $D = 3$ and $D = 2$ give [12, 13]

$$\mathrm{Gi}_{3D} = \frac{1}{32\pi^2}\frac{T_{c0}b_\psi^2}{a_\psi'\mathcal{H}_\psi^3}, \quad \mathrm{Gi}_{2D} = \frac{1}{4\pi}\frac{b_\psi n_z}{a_\psi'\mathcal{H}_\psi}, \qquad (19)$$

where $a_\psi' \equiv da_\psi/dT$, and the fact the system is isotropic implies equality of the coefficients of the gradient terms $\mathcal{H}_\psi = \mathcal{H}_\psi^{(i)}$. In the case of $D = 2$, one has degeneracy along the z direction, and we introduce a factor n_z that takes into account the density of states along this direction. The transition to the anisotropic case in the expressions ((19)) is carried out by replacing $\mathcal{H}_\psi^3 \to \mathcal{H}_\psi^{(x)}\mathcal{H}_\psi^{(y)}\mathcal{H}_\psi^{(z)}$ for $D = 3$ and $\mathcal{H}_\psi$ to $\sqrt{\mathcal{H}_\psi^{(x)}\mathcal{H}_\psi^{(y)}}$ for $D = 2$.

The assumption $T_c \sim T_{Gi}$ gives a rough estimate of the fluctuation-induced shift of the transition temperature $\delta T_c = T_{c0} - T_c$. More accurate calculations of the relationship between δT_c and the Ginzburg number can be made, for example, using renormalization group approach for a one-component energy functional (13) [13]. In the case of $D = 2$, the Nelson–Kosterlitz criterion can be applied, which connects the temperature of the Berezinsky–Kosterlitz–Thouless phase transition [43] with the Ginzburg number. Below we will examine in detail the important examples when the two-band system under consideration has (1) quasi-one-dimensional (Q1D) and three-dimensional bands (3D), (2) quasi-one-dimensional and quasi-two-dimensional bands (Q1D + Q2D) and (3) two quasi-two-dimensional bands (Q2D + Q2D).

3.2. Q1D + 3D

The general mechanism for suppressing fluctuations and increasing the critical temperature is manifested especially clearly when the system has a quasi-one-dimensional (Q1D) band. Quasi-one-dimensional bands are characterized by diverging van Hove singularities of the single particle density of states (DOS) at the band edges. If the chemical potential is found near the singularity, which takes place, for example, when the system is near the Lifshitz transition, then this leads to a high DOS at the Fermi surface and, accordingly, to high values of the mean-field critical temperature T_{c0}. The size of Cooper pairs in this band decreases sharply and, thus, the BCS–BEC crossover regime is reached. However, large fluctuations in the Q1D system suppress superconductivity completely.

It turns out that coupling with the 3D band can suppress fluctuations and restore superconductivity. Indeed, with such interaction between the bands, the contribution of fluctuations is determined by the effective 3D functional (13), where the coefficients are given by Eqs. (14). In these expressions, the band coefficients for a three-dimensional BCS-type band with a spherically symmetric Fermi surface are given by standard expressions [44]

$$\mathcal{A}_1 = N_1 \ln\left(\frac{2e^\gamma\hbar\omega_c}{\pi T_{c0}}\right), \quad a_1 = \frac{N_1}{T_{c0}}(T - T_{c0}),$$

$$b_1 = \frac{7\zeta(3)}{8\pi^2}\frac{N_1}{T_{c0}^2}, \quad \mathcal{H}_1^{(i)} = \mathcal{H}_1 = \frac{\hbar^2 v_1^2}{6}b_1, \qquad (20)$$

where the isotropy of the system, as indicated above, means the equality of the coefficients $\mathcal{H}_1^{(i)}$ for all directions i, N_1 denotes the density of states of the band $\nu = 1$, $\hbar\omega_c$ is the energy cutoff (we will further take it as the energy scale for all energy quantities), γ is the Euler's constant, $\zeta(x)$ is the Riemann zeta function, and the characteristic velocity of electrons is equal to the Fermi velocity $v_1 = \sqrt{2(\mu - \epsilon_{0,1})/m_1}$, where m_ν is the effective mass.

For the Q1D band, we assume that the chemical potential is found near its edge, and therefore the coefficients are expressed as integrals to be calculated numerically,

$$\mathcal{A}_2 = N_2\int_{-\tilde{\mu}}^{1} dy\frac{(y/2\tilde{T}_{c0})}{y\sqrt{y+\tilde{\mu}}},$$

$$a_2 = -\tau\frac{N_2}{2\tilde{T}_{c0}}\int_{-\tilde{\mu}}^{1} dy\frac{\mathrm{sch}^2(y/2\tilde{T}_{c0})}{\sqrt{y+\tilde{\mu}}},$$

$$b_2 = \frac{N_2}{4\hbar^2\omega_c^2}\int_{-\tilde{\mu}}^{1} dy\frac{\mathrm{sch}^2(y/2\tilde{T}_{c0})}{y^3\sqrt{y+\tilde{\mu}}}\left[\sinh\left(\frac{y}{\tilde{T}_{c0}}\right) - \frac{y}{\tilde{T}_{c0}}\right],$$

$$\mathcal{H}_2^{(x)} = \hbar^2 v_2^2\frac{N_2}{8\hbar^2\omega_c^2}\int_{-\tilde{\mu}}^{1} dy\frac{\sqrt{y+\tilde{\mu}}}{y^3}\mathrm{sch}^2(y/2\tilde{T}_{c0})$$

$$\times\left[\sinh\left(\frac{y}{\tilde{T}_{c0}}\right) - \frac{y}{\tilde{T}_{c0}}\right], \quad \mathcal{H}_2^{(y)} = \mathcal{H}_2^{(z)} = 0, \qquad (21)$$

where we introduced a quantity describing the proximity to the transition temperature $\tau = 1 - T/T_{c0}$, and also, for convenience, use dimensionless variables

$\tilde{T}_{c0} = T_{c0}/\hbar\omega_c$ and $\tilde{\mu} = \mu/\hbar\omega_c$. Note that the effective velocity v_2 and the density of states N_2 in the expressions for the Q1D band are determined by the energy cutoff value, $v_2 = \sqrt{2\hbar\omega_c/m_2}$ and $N_2 = n_y n_z/4\pi\hbar v_2$. Here we assume that the contribution of the y and z directions to the single-particle DOS of the Q1D band is described by constants n_y and n_z that are specified by the dimensions of the Brillouin zone. Since the band $\nu = 2$ is quasi-one-dimensional, then $\mathcal{K}_\psi^{(y,z)} \neq \mathcal{K}_\psi^{(x)}$ and, therefore, the functional (13) is anisotropic.

In the following, we will use the well-known result obtained by means of the renormalization group calculations [13], according to which the fluctuation shift of the critical temperature for the three-dimensional GL functional (13) is equal to

$$\frac{T_{c0} - T_c}{T_c} = \frac{8}{\pi}\sqrt{\mathrm{Gi}}, \tag{22}$$

where the Ginzburg number for a three-dimensional anisotropic superconductor is given by (see explanation after Eq. (19))

$$\mathrm{Gi} = \frac{1}{32\pi^2}\frac{T_{c0}b_\psi^2}{a'_\psi \mathcal{K}_\psi^{(x)}\mathcal{K}_\psi^{(y)}\mathcal{K}_\psi^{(z)}}. \tag{23}$$

It is convenient to represent this expression in the form

$$\mathrm{Gi} = \mathrm{Gi}_1 \frac{(1 + S^4 b_2/b_1)^2}{(1 + S^2 a_2/a_1)(1 + S^2\mathcal{K}_2^{(x)}/\mathcal{K}_1^{(x)})}, \tag{24}$$

where Gi_1 is the Ginzburg number for the 3D band $\nu = 1$ given by Eq. (19), in which the coefficients $a'_\psi, b_\psi, \mathcal{K}_\psi$ are replaced by $a'_1, b_1, \mathcal{K}_1$, so that

$$\mathrm{Gi}_1 = \frac{1}{32\pi^2}\frac{T_{c0}b_1^2}{a'_1\mathcal{K}_1^3} = \frac{27\pi^4}{14\zeta(3)}\left(\frac{T_{c0}}{\mu + |\epsilon_0|}\right)^4. \tag{25}$$

We can quantify the value of this expression as $\mathrm{Gi}_1 = 10^{-10}$, which roughly corresponds to the middle of the interval typical for three-dimensional superconductors $\mathrm{Gi}_{3D} \simeq 10^{-16}$–$10^{-6}$ [12]. The ratio N_2/N_1 is assumed unity, which is close to experimental estimates for many multiband superconducting materials (see, e.g., references in [45]). We have to set values of the intra- and interband interactions g_{11}, g_{22}, and g_{12}, which determine the critical temperature. Note that for the calculations it is convenient to introduce dimensionless interaction constants $\lambda_{\nu\nu'} = g_{\nu\nu'}\sqrt{N_\nu N_{\nu'}}$.

Figure 3a shows a typical dependence of critical temperatures T_{c0} and T_c on the chemical potential near the bottom of a quasi-one-dimensional band, calculated in [33, 34, 37]. The calculations were performed at $\lambda_{11} = 0.18$ and $\lambda_{22} = 0.2$, however, obtained dependencies remains qualitatively similar for other

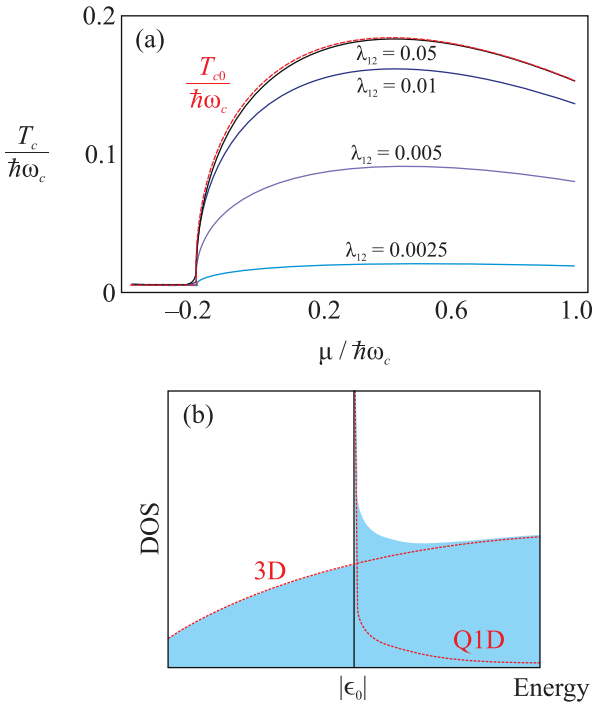

Fig. 3. (Color online) (a) Critical temperature taking into account fluctuations as a function of chemical potential for interband couplings $\lambda_{12} = 0.0025$; 0.005; 0.01; 0.05 at $\lambda_{11} = 0.18$; $\lambda_{22} = 0.2$. The red dashed line shows the critical temperature T_{c0}. (b) Schematic representation of the dependence of the density of states in a two-band 3D + Q1D system. The red dashed lines show the density of states of non-interacting bands. Adapted from [33]. By courtesy of American Physical Society.Key: 1. Energy

values of the intraband coupling constants typically found in conventional superconductors [44]. The values of the interband coupling constant λ_{12} are chosen to be $\lambda_{12} < 0.05$, taking into account that the relation $\lambda_{12} \ll \lambda_{11}, \lambda_{22}$ is usually found for many two-band superconductors (see, for example, the table of interaction constants in [45]). The chemical potential varies near the edge of the Q1D band, crossing it at $\mu = 0$.

Figure 3a shows that at sufficiently low values of the chemical potential ($\mu \lesssim -0.2$) there is no contribution from the Q1D band. In this case, T_{c0} is determined by the three-dimensional band and is sufficiently low, as in traditional superconducting materials. As the chemical potential approaches the bottom of the Q1D band ($\mu \simeq 0$), T_{c0} increases sharply due to the van Hove singularity in the DOS, see Fig. 3b.

Note that the increase in T_{c0} takes place before the chemical potential touches the edge of the Q1D band, at $\mu \simeq -0.2$. This is due, firstly, to the influence of the binding energy of Cooper pairs, which in the region of increasing critical temperature can be estimated as

$\max(T_{c0}) \simeq 0.2$, and which blurs the Fermi surface. Moreover, at finite temperatures there is also a temperature-induced blurring of the Fermi surface, which is also controlled by the value $\max(T_{c0}) \simeq 0.2$. For large values of the chemical potential ($\mu > \hbar\omega_c$), the influence of the singularity in the DOS is less significant, and T_{c0} decreases when μ rises as $1/\sqrt{\mu}$ (which is typical for Q1D band) until it reaches the value determined by the 3D band. In the Figure 3a, the dependence of T_{c0} on μ is shown for $\lambda_{12} = 0.05$. However, this dependence remains practically unchanged throughout the entire considered interval of the coupling constants $\lambda_{12} \ll \lambda_{11}, \lambda_{22}$. Consequently, for those values of the interband interaction, the properties of a two-band superconductor calculated within the framework of the mean field theory are fully determined by the Q1D band.

In contrast, the dependence of the critical temperature T_c, which takes into account the fluctuation-induced shift, depends on λ_{12} strongly. Indeed, when the interband coupling is "turned off" ($\lambda_{12} \to 0$) the fluctuations suppress superconductivity. The situation changes as λ_{12} increases. In is clear from Fig. 3a that even an extremely small interband coupling $\lambda_{12} \simeq 0.01$ allows T_c to be brought almost to its field-average value of T_{c0}.

This calculation shows that the inter-band coupling to a stable three-dimensional condensate makes it possible to suppress strong fluctuations inherent in quasi-one-dimensional systems. Despite the fact that in real systems the band structure may be somewhat different from the ones shown in Fig. 2, weakening the fluctuations suppression effect, the considered mechanism is physically general and can lead to a significant increase in the critical temperature of the superconducting transition, if the system chemical potential is located near the edge of the quasi-one-dimensional band.

3.3. Q1D + Q2D

It is known that fluctuations increase in low-dimensional systems [13]. Therefore, one expects the mechanism for suppressing the fluctuations, discussed in the previous section for a two-band system with 3D and Q1D bands, will be much less effective if a superconductor has a quasi-two-dimensional band (Q2D). In this section, we consider a system with deep Q2D and shallow Q1D bands and show that the fluctuations suppression mechanism remains almost as effective as in the previous case with a 3D band.

For the Q1D band ($\nu = 2$), the expansion coefficients of the free energy functional (5) are given in the equation (21), and for the deep Q2D band ($\nu = 1$) the following expressions can be obtained [46],

$$\mathcal{A}_1 = N_1 \ln\left(\frac{2e^{\gamma}\hbar\omega_c}{\pi T_{c0}}\right), \quad a_1 = \frac{N_1}{T_{c0}}(T - T_{c0}),$$

$$b_1 = \frac{7\zeta(3)}{8\pi^2}\frac{N_1}{T_{c0}^2}, \quad \mathcal{K}_1^{(x,y)} = \mathcal{K}_1 = \frac{7\zeta(3)}{32\pi^2}\frac{N_1\hbar^2 v_1^2}{T_{c0}^2}, \quad (26)$$

where N_1 is the DOS of the 2D band, which includes the factor n_z due to degeneracy along the z axis (for the Q1D band we have the same factor n_z and n_y to take into account the direction y), $v_1 = \sqrt{2(\mu - \epsilon_{0,1})/m_1}$, and $\mathcal{K}_1^{(z)} = 0$.

The corresponding Ginzburg number for an anisotropic two-band system can be written as (see explanation after Eq. (19))

$$\mathrm{Gi} = \frac{T_{c0} b_\psi n_z}{4\pi a'_\psi \sqrt{\mathcal{K}_\psi^{(x)}\mathcal{K}_\psi^{(y)}}}. \quad (27)$$

As in the previous case, we take into account that the coefficients of the functional (14) contain the contribution of both bands, and we rewrite the Ginzburg number for a two-band system (27) in the form

$$\mathrm{Gi} = \mathrm{Gi}_1 \frac{1 + S^4 b_2/b_1}{(1 + S^2 a'_2/a'_1)\sqrt{1 + S^2\mathcal{K}_2^{(x)}/\mathcal{K}_1^{(x)}}}, \quad (28)$$

where Gi_1 is the Ginzburg number of the deep Q2D band $\nu = 1$, which is obtained from Eq. (27) by replacing the coefficients $a'_\psi, b_\psi, \mathcal{K}_\psi$ with $a'_1, b_1, \mathcal{K}_1$. After this replacement one obtains

$$\mathrm{Gi}_1 = \frac{T_{c0} b_1 n_z}{4\pi a'_1 \mathcal{K}_1^2} = \frac{T_{c0}}{\mu + |\epsilon_0|}. \quad (29)$$

Since $b_1 \propto n_z, a'_1 \propto n_z$ and $\mathcal{K}_1^{(i)} \propto n_z$, the value of the Ginzburg number does not depend on the factor n_z.

To calculate T_c of our effective Q2D system, we can use the Nelson–Kosterlitz criterion [43] according to which the fluctuation-induced shift of the critical temperature is calculated as

$$\frac{T_{c0} - T_c}{T_c} = 4\mathrm{Gi}, \quad (30)$$

where T_c is the temperature of the Berezinsky–Kosterlitz–Thouless [47] phase transition. Alternatively, one can use the renormalization group approach, which gives for $D = 2$ [13]

$$\frac{T_{c0} - T_c}{T_c} = 2\mathrm{Gi}\ln(1/4\mathrm{Gi}). \quad (31)$$

It is important to emphasize that the difference between the results in Eqs. (31) and (30) becomes significant only when $\delta T_c/T_c \lesssim 0.001$, so that when T_c and T_{c0} are practically indistinguishable. In addition, the expression (31) is valid only for (T_{c0} –

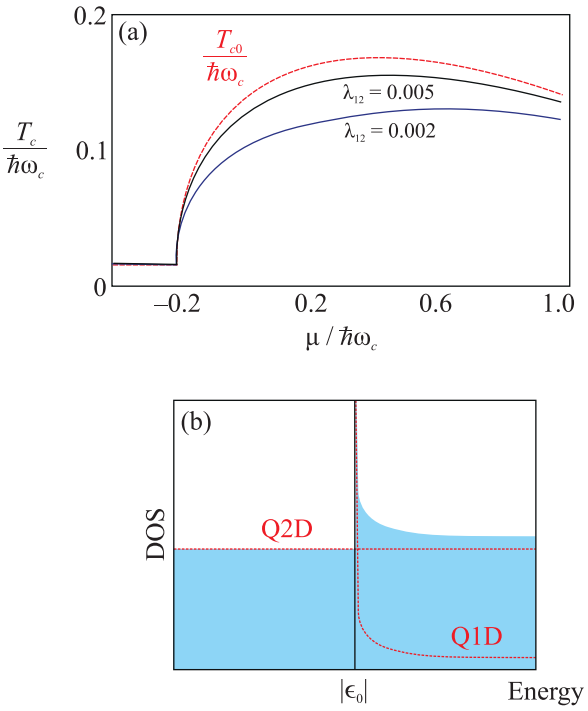

Fig. 4. (Color online) (a) Critical temperature taking into account fluctuations as a function of chemical potential, calculated for interband couplings $\lambda_{12} = 0.002; 0.005$ at $\lambda_{11} = 0.24$; $\lambda_{22} = 0.2$. The red dashed line shows the mean field critical temperature T_{c0}. The ratio of effective masses in two bands is $m_2/m_1 = 1$. (b) Schematic representation of the dependence of the density of states in a two-band Q2D + Q1D system. The red dashed lines show the densities of states of non-interacting bands. Adapted from [34]. By courtesy of American Physical Society.

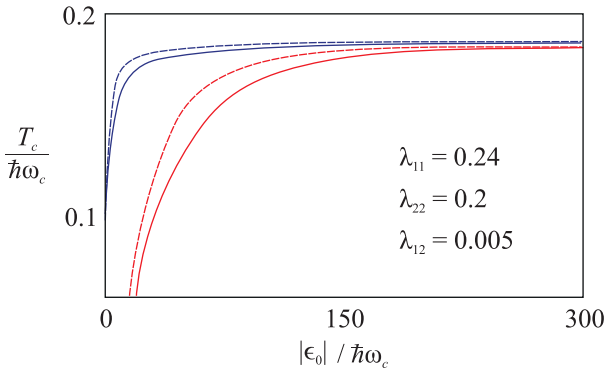

Fig. 5. (Color online) Critical temperature taking into account fluctuations depending on the depth of the $|\epsilon_0|$ high-dimensional band. The results for the Q1D + 3D system are shown in blue, and the results for the Q1D + Q2D system in red. Solid lines correspond to equal effective masses of carriers in the bands, dashed lines correspond to the mass ratio $m_1/m_2 = 4$, $\mu = 0.4$. Adapted from [34]. By courtesy of American Physical Society.

$T_c)/T_c \lesssim 0.1$. Both approaches for calculating T_c are used below, which lead to very similar results. In particular, Figs. 4 and 5 are obtained using the Eq. (30), while the results presented in the next section in Fig. 6 are based on Eq. (31).

Figure 4a shows the dependence of T_{c0} and T_c calculated using Eq. (30) as functions of the chemical potential for the intraband coupling $\lambda_{11} = 0.24$, $\lambda_{22} = 0.2$, and the interband coupling constants $\lambda_{12} = 0.002$ and 0.005. The depth of the quasi-two-dimensional band $\nu = 1$ is chosen as $|\epsilon_0| = 300$, which sets the Fermi energy of this band $E_F \approx 300$, since $\mu \ll |\epsilon_0|$. This Fermi energy value corresponds to realistic microscopic parameters for traditional single-element superconductors [48]. For example, for aluminum $E_F \approx 350$, and for lead $E_F \approx 1000$.

Despite the general trend of increasing fluctuations when the system dimensionality decreases, a comparison of Figs. 3 and 4 shows that for the mechanism of suppression of superconducting fluctuations considered in this work, a decrease in the dimensionality of the deep band from $D = 3$ to $D = 2$ does not play a significant role. The difference between T_c for the Q1D + 3D and Q1D + Q2D systems reaches a value of only 30%, when the chemical potential changes in the interval of $\mu = 0.2 \div 0.6$. This relatively weak dependence of T_c on the dimensionality of the band $\nu = 1$ takes place due a similar DOS (cf. Figs. 3b and 4b), and also due to the dependence of $(T_{c0} - T_c)/T_c$ on the Ginzburg number. Despite that the Ginzburg number for a 2D band Gi_{2D} is orders of magnitude larger than that for the 3D band Gi_{3D}, the shift of the critical temperature according to Eq. ((30)) depends linearly on Gi_{2D} in the Q2D system, and depends as the square root of Gi_{3D} for the 3D system in Eq. (22). This makes the shift $T_{c0} - T_c$ comparable for the two systems.

The above results were obtained under the assumption of $|\epsilon_0| \gg \hbar\omega_c$, which is typical in conventional single-component superconductors. In multiband superconducting compounds, the Fermi energy can be one or two orders of magnitude lower than this value, $E_F \lesssim 10\hbar\omega_c$ [17, 18, 21].

Figure 5 shows the dependence of the critical temperature T_c, with the account for fluctuations, on the depth of the $\nu = 1$ band, calculated for the value of the chemical potential corresponding to the maximum of T_c (Eq. (30) is used). For small values of $|\epsilon_0|$ the critical temperature is quite different from the mean field value $T_{c0} \approx 0.18$. However, T_c quickly approaches T_{c0} when $|\epsilon_0|$ increases. The reason for the strong difference between T_c and T_{c0} at small $|\epsilon_0|$ is a decrease in the coherence length in deep band $\nu = 1$, which leads to an increase in Gi_1 and, accordingly, an increase in the fluctuations in this band.

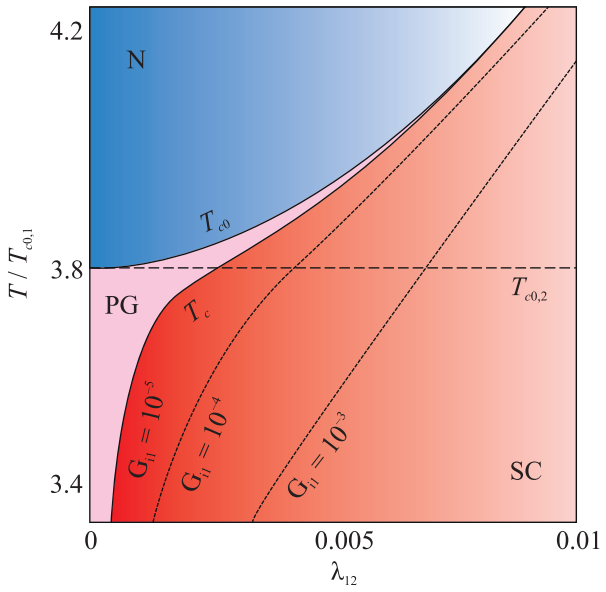

Fig. 6. (Color online) Phase diagram on the $T - \lambda_{12}$ plane and the critical temperature of the superconducting transition, calculated in the mean field approximation (T_{c0}) and taking into account fluctuations (T_c), as a function of the interband interaction amplitude λ_{12} for a superconductor with two quasi-two-dimensional bands. Red color denotes the superconducting state SC ($T < T_c$), blue color corresponds to the normal state N ($T < T_{c0}$), and pink color shows the region of pair fluctuations PG ($T_c < T < T_{c0}$). The dependence $T_c(\lambda_{12})$ is shown for various values of the Ginzburg number of the deep band $\nu = 1$. The horizontal dashed line shows the mean field critical temperature in the shallow band $\nu = 2$ in the absence of pairing. Adapted from [36]. By courtesy of American Physical Society.

The dashed lines in Fig. 5 show the same dependence $T_c(|\epsilon_0|)$, but calculated for different effective masses of carriers in the bands, $m_1/m_2 = 4$. It can be seen that varying the effective mass ratio changes the dependencies only quantitatively, slightly shifting the domain of strong fluctuations towards the lower values of $|\epsilon_0|$.

3.4. Q2D + Q2D

The case of interaction of two quasi-two-dimensional bands is also very interesting, since the Fermi surfaces of many multiband materials have a quasi-two-dimensional character [18]. As before, we assume that one of these bands ($\nu = 1$) is deep, and the other ($\nu = 2$) is shallow. In this situation, there is not a significant increase in the DOS near the edge of the shallow band. However, the shallow band condensate can also be in the BCS–BEC crossover regime, and the mechanism for suppressing fluctuations and stabilizing the crossover will be effective under the condition of weak coupling with the deep band.

For the deep Q2D band $\nu = 1$, the expansion coefficients in the energy functional (5) are given in the Eq. (26). For a shallow Q2D band $\nu = 2$ they have the same form for all the coefficients of the functional, with the exception of the gradient term, which in this case reads as [46]

$$\mathcal{K}_2 = \frac{3\zeta(2)}{8\pi^2}\frac{N_2\hbar^2 v_2^2}{T_{c0}^2}, \tag{32}$$

where, as before, N_2 denotes the DOS of this band, and the characteristic velocity $v_2 = \sqrt{2T_{c0}/m_2}$ is determined by the critical temperature.

Note that in this case we can explicitly find a solution to the Eq. (7) for the mean-field critical temperature [49]:

$$T_{c0} = \frac{2e^{\gamma}}{\pi}\hbar\omega_c \exp\left[-\frac{\lambda_{22} - \lambda_{12}\chi^{1/2}S}{\lambda_{11}\lambda_{22} - \lambda_{12}^2}\right], \tag{33}$$

where $\chi = N_2/N_1$, $\lambda_{\nu\nu'} = g_{\nu\nu'}\sqrt{N_\nu N_{\nu'}}$, and the value S found from Eq. (7) and (9) can be conveniently rewritten in the form of

$$S = \frac{\chi^{-1/2}}{2\lambda_{12}}[\lambda_{22} - \lambda_{11} + \sqrt{(\lambda_{22} - \lambda_{11})^2 + 4\lambda_{12}^2}]. \tag{34}$$

The fluctuation-induced shift of the critical temperature is found using Eq. (31). The Ginzburg number for the effective Q2D system is given by Eq. (27), which can be written, similarly to Eq. (28), as

$$\mathrm{Gi} = \mathrm{Gi}_1 \frac{1 + S^4 b_2/b_1}{(1 + S^2 a_2'/a_1')}\frac{1}{\sqrt{1 + S^2\mathcal{K}_2^{(x)}/\mathcal{K}_1^{(x)}}} \times \frac{1}{\sqrt{1 + S^2\mathcal{K}_2^{(y)}/\mathcal{K}_1^{(y)}}}, \tag{35}$$

where, as before, Gi_1 is the Ginzburg number for the deep Q2D band.

Numerical results for the obtained expressions, performed in the limit of $v_2 \gg v_1$ for parameters $\lambda_{11} = 0.12$, $\lambda_{22} = 0.15$ and $N_1 = N_2$, are shown in Fig. 6. The Fig. 6 shows a color phase diagram of the state of the system on the λ_{12}–T plane (the temperature is given relative to the deep band transition temperature $T_{c0,1}$ calculated in the absence of the interband coupling). In the diagram in Fig. 6, the lines show T_{c0} and T_c as functions of λ_{12}. The latter are calculated for several values of Gi_1 for the deep band. The red color denotes the superconducting state *SC* ($T < T_c$), the blue color marks the normal state *N* ($T > T_{c0}$), and the pink is the region of strong fluctuations or pseudogap (PG) ($T_{c0} < T < T_c$).

The results show that in this case too, fluctuations are almost completely suppressed even at extremely small values of the interband coupling constant λ_{12}. Just as before, this effect is more pronounced the

weaker the amplitude of fluctuations in the deep band. For example, for a deep band with the Ginzburg number $\mathrm{Gi}_1 = 10^{-5}$, the PG region becomes negligible at $\lambda_{12} \gtrsim 0.001$, and the critical temperature T_c is almost equal to mean field critical temperature of the shallow band $T_{c0.2}$. Note that the estimate of the interband coupling interval for multiband superconducting materials gives $0.005 \lesssim \lambda_{12} \lesssim 0.4$ [45].

3.5. Fluctuations of the Magnetic Field

To conclude this section, we mention that in addition to fluctuations of the order parameter, it is also necessary to take into account fluctuations of the magnetic field. The calculation of the corresponding contributions to the fluctuation-induced shift of the critical temperature was reported in [50]. The results show that the shift of the critical temperature (22) for the 3D band acquires an additional contribution

$$\frac{T_{c0} - T_c}{T_c} = \frac{8}{\pi}\sqrt{\mathrm{Gi}} + \frac{4}{\pi\kappa^2}\sqrt{\mathrm{Gi}}. \qquad (36)$$

Consequently, taking into account the field-induced fluctuations does not lead to a change in the square root dependence of the shift on Gi, changing only its pre-factor.

For a 2D system, taking into account the field fluctuations by the renormalization group approach yields the following expression for the shift of the critical temperature

$$\frac{T_{c0} - T_c}{T_c} = 2\mathrm{Gi}\ln\frac{1}{4\mathrm{Gi}} + \frac{\mathrm{Gi}}{2\kappa^2}\ln\frac{1+y}{\mathrm{Gi}+y}, \qquad (37)$$

where Gi is the Ginzburg parameter for the 2D band, y is calculated as

$$y = \frac{\mathrm{Gi}}{\kappa^2}\ln\frac{1}{\mathrm{Gi}}, \qquad (38)$$

and κ is the Ginzburg–Landau parameter. This is a more complex expression than Eq. (31). Nevertheless, taking into account the fact that for small values of Gi $y \ll 1$, we find that in this case the main contribution to the shift of the critical temperature has the same functional dependence on Gi as the expression (31), only with a different numerical coefficient.

Therefore, taking into account field fluctuations increases the shift in the critical temperature only slightly. This, however, does not change the main conclusion that interaction of band condensates gives rise to an effective suppression of fluctuations. Note that from Eqs. (36) and (37) it is clear that the field fluctuations are negligible for type II superconductors with $\kappa \gg 1$.

4. MATERIALS

In the previous sections it was shown that when a superconductor has two interacting single-particle bands, "shallow" and "deep", one expects a strong suppression of superconductive fluctuations and, thus, stabilizing the BCS–BEC crossover mode in the shallow band. This could possibly give rise to a significant enhance in the critical temperature of the superconducting transition. The enhancement takes place if the shallow band has an increased DOS, for example, due to the van Hove singularity in a quasi-one-dimensional band. The singularity of the DOS leads to a sharp increase in the mean-field critical temperature corresponding to creating Cooper pairs in this band, while its interaction with the deep band suppresses the fluctuations. An essential ingredient of this mechanism is that it becomes effective even if the interband coupling is very weak. Note that an increase in the DOS is also possible if there is a flat band in the system.

The mechanism is not very sensitive to the details of the band structure and can take place in various materials, as long as their band structure satisfies the conditions described above. Currently, there are quite a few compounds in which these requirements can be satisfied.

4.1. Quasi-one-dimensional Materials

Obvious candidates for the implementation of the above mechanism are materials with a pronounced quasi-one-dimensional structure, and, accordingly, with a singularity in the density of states. It is well known that in purely one-dimensional systems with short-range interactions, thermal and quantum fluctuations prevent the formation of the long-range order at finite temperatures, which is an obstacle to the emergence of superconductivity. The situation changes if there is a transverse interaction between individual one-dimensional systems, i.e., the entire system as a whole is quasi-one-dimensional. Examples of such quasi-one-dimensional superconducting systems are Bechgaard salts $(\mathrm{TMTSF})_2\mathrm{X}$ [16], structures based on molybdenum selenide $M_2\mathrm{Mo}_6\mathrm{Se}_6$ (M = Tl,In) [53], lithium-molybdenum bronze $\mathrm{Li}_{0.9}\mathrm{Mo}_6\mathrm{O}_{17}$ [54].

In the light of the suppressing fluctuations mechanism, discussed above, it is the transverse interaction between one-dimensional structures that leads to the formation of higher-dimensional electronic bands. The interaction suppresses the fluctuations in quasi-one-dimensional bands and ensures the appearance of superconductivity in the system. It seems this mechanism is fully realized in chromium pnictides

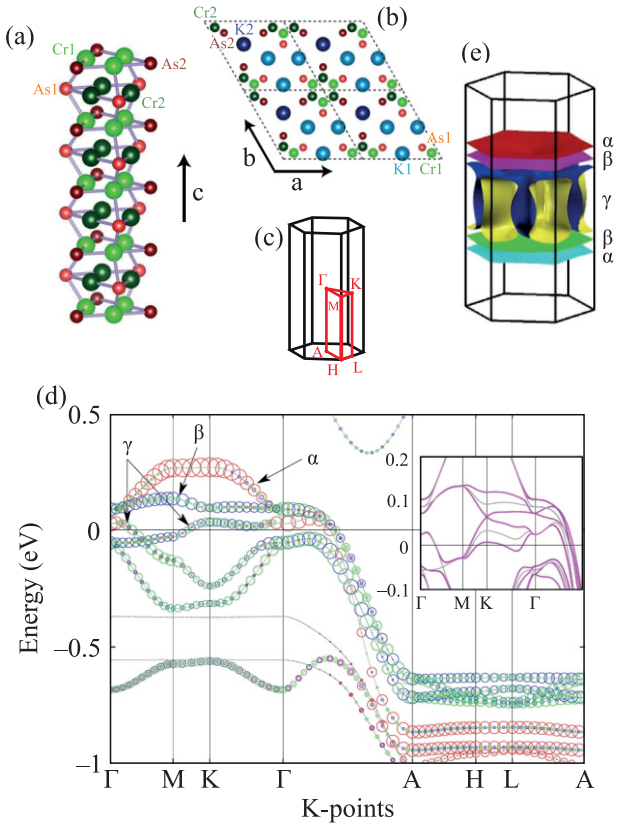

Fig. 7. (Color online) Crystal and band structure of the quasi-one-dimensional superconductor $K_2Cr_3As_3$. (a) Double-walled subnanotube $[(Cr_3As_3)^{2-}]_\infty$; (b) Top view of four unit cells. Adapted from [51]. (c) First Brillouin zone. (d) Band structure. The inset shows a comparison of relativistic (purple lines) and non-relativistic (gray lines) results. The size of the red, blue and green circles is proportional to the contributions of the $d_{z^2}, d_{x^2-y^2}$ and d_{xy} orbitals, respectively. Orbitals having states near the Fermi surface are designated by the letters α, β, γ; (e) Fermi surface consisting of two quasi-one-dimensional (α, β) and one three-dimensional (γ) sheets. Adapted from [52].

$M_2Cr_3As_3$, (M = K,Rb,Cs), a family of materials in which superconductivity was discovered in 2015 [55–57].

At room temperature $K_2Cr_3As_3$ has a hexagonal crystal lattice with constants $a = 9.98A$ and $c = 4.23A$ (see Figs. 7a and 7b). The featured structural units of this crystal are one-dimensional negatively charged "chains" $[(Cr_3As_3)^{2-}]_\infty$, which are subnanotubes with double walls that have an outer diameter of 0.58 nm. These subnanotubes are well separated from each other by chains of potassium counter-ions. As a result, the interaction between individual subnanotubes is significantly weaker compared to the interactions within the subnanotube. In this respect, this material is truly quasi-one-dimensional.

First-principles calculations (Figs. 7c–7e) show that single-particle states near the Fermi energy are occupied mainly by chromium $3d$-electrons, and the Fermi surface comprises two Q1D and one 3D sheets. The same type of the band structure is characteristic of other members of the family of such compounds; in addition, $Cs_2Cr_3As_3$ has one more Q1D sheet on the Fermi surface [58].

The temperature of the superconducting transition decreases when replacing potassium in the compound with heavier elements. If for $K_2Cr_3As_3$ $T_c = 6.1$ K, then for $Rb_2Cr_3As_3$ it is 4.8 K [56], and only 2.2 K for $Cs_2Cr_3As_3$ [57]. The change in the critical temperature is explained by different distances between subnanotubes in these compounds. In the compounds based on rubidium and chromium, this distance is, respectively, 3 and 6% larger compared to the compound based on potassium. This leads to a weakening of the interaction between subnanotubes and, as a consequence, to a decrease in the critical temperature.

Further experiments with the above-mentioned quasi-one-dimensional multiband superconductors aiming to tune the chemical potential to achieve conditions for a significant increase in the critical temperature appear very promising. This tuning can be achieved in a variety of ways, such as chemical engineering, high pressure, or doping. In this regard, it is worth mentioning the recent very interesting results of the ab initio calculations that demonstrated the possibility of observing the Lifshitz transition in $KCr_3As_3H_x$ when one changes the hydrogen intercalation [60].

4.2. Iron-Based Superconductors

At present, iron-based superconductors appear to be the most promising systems for implementing the multi-band fluctuations suppression mechanism. A few investigations have also attempted to explain atypical properties of cuprate HTSCs by the presence of BCS–BEC crossover manifested by the large band gaps and low charge carrier concentrations in these compounds (see, for example, [61]). However, apparently, superconductivity in cuprate HTSCs has a different nature [62].

4.2.1. FeSe Monolayers. As already mentioned in the Section 2 in the BEC regime (or strong coupling regime), the mean field temperature T_{c0} of the pair formation and the real superconducting transition temperature T_c are clearly different. In the range between T_{c0} and T_c, Cooper pairs also exist, creating large superconducting fluctuations and depleting the low-energy density of states, which results in the formation of a pseudogap.

FeSe monolayers have very small hole and electron pockets on the Fermi surface, and their ratio of the superconducting energy gap to the Fermi energy reaches values of $\Delta/E_F \approx 0.3$–1.0 [20, 63]. These val-

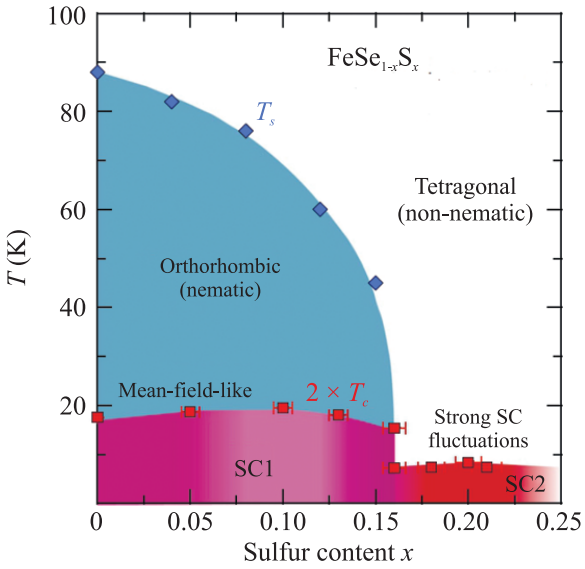

Fig. 8. (Color online) Experimentally obtained phase diagram for the compound $FeSe_{1-x}S_x$ in the coordinates "doping level–temperature". Red squares and blue diamonds correspond to the temperatures T_c of superconducting and T_s of nematic phase transitions, respectively. At a critical doping level $x_c \approx 0.17$, a sharp jump in T_c occurs, indicating a restructuring of the ground state of the superconducting phase. Adapted from [24]. Creative Commons Attribution 4.0 International License.

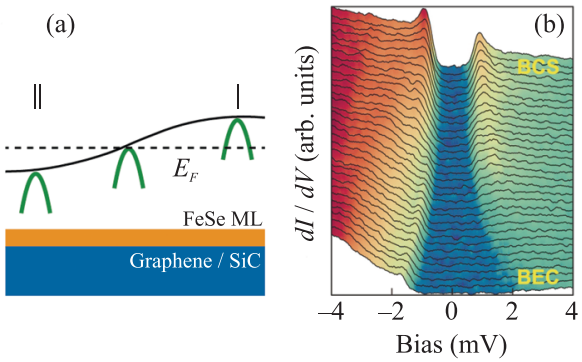

Fig. 9. (Color online) Realization of BCS–BEC crossover in real space in a FeSe monolayer on a graphene substrate. (a) Shift of the band structure relative to the Fermi level (dashed line) caused by different ordering of the graphene layers in the substrate. Region I corresponds to BCS, and region II to BEC. (b) Spatially resolved dI/dV spectrum measured along the dashed line in panel (a). Adapted from [59].

ues correspond to the BCS–BEC crossover regime. On the other hand, scanning tunneling spectroscopy measurements did not detect the formation of a pseudogap above T_c [21].

These results imply that superconductivity in FeSe is not described as a conventional BCS–BEC transition. An important aspect is the influence of the multiband electronic structure, which, in addition to the Δ/E_F ratio, may have other factors affecting the properties of the crossover.

In the work [24], measurements of the heat capacity and magnetic torque, as well as high-resolution scanning tunneling spectroscopy revealed the phase diagram of a sulfur-doped FeSe monolayer as a function of the doping level (Fig. 8). The form of the phase diagram indicates that the superconducting transition is not described by the mean field theory. One of the main results of the experiment is the absence of a pseudogap in the STS spectra at temperatures above T_c. It is assumed that the key factors determining the properties of the crossover in $FeSe_{1-x}S_x$ are the multiband nature of the Fermi surface, as well as the proximity to the Lifshitz transition, which takes place at the critical doping $x_c \approx 0.17$.

FeSe monolayers appear a very promising system for implementing BCS–BEC crossover because the Fermi energy in this compound is only a few meV and can be accurately and relatively easily tuned by the changing the number of layers of the graphene substrate [22], as well as by varying the geometry of their ordering. In [23], the crossover was achieved in a FeSe monolayer placed on a three-layer graphene substrate, where the layers ordering was different in different places of the substrate (ABA and ABC). This led to spatial changes in the work function in graphene, which caused a shift in the peak of the hole dispersion curve in FeSe (Fig. 9a). The single particle DOS, measured along the dashed line in the diagram using scanning tunneling spectroscopy, has a gap in region I of the sample. The gap reveals the electron-hole symmetry characteristic of the BCS superconductor. When moving from region I to region II, the electron-hole symmetry is broken, and the DOS takes the form of a step function characteristic of the crossover [64]. It is reported that the value of $\Delta/E_F \simeq 0.3$ was achieved.

4.2.2. Bulk samples. In [17], using angle-resolved photoelectron spectroscopy, it was first discovered that compounds based on FeSe, namely, $FeSe_xTe_{1-x}$ reveal the presence of a BCS–BEC crossover.

Figure 10 shows the dispersion dependence of one of the bands near the Fermi level $E_F = 4 \pm 2.5$ meV, measured at temperatures corresponding to the normal and superconducting states of the sample. The dispersion curve far from the Fermi level was obtained from the momentum distribution (marked with red dots in Fig. 10). It is identical at temperatures $T = 8\ \text{K} < T_c$ and $T = 15\ \text{K} > T_c$ and is well approximated by a quadratic dependence (shown by the red line). In the region of low energies and low temperatures, the dispersion was obtained from the energy distribution (black dots in Fig. 10). The minimum gap was discov-

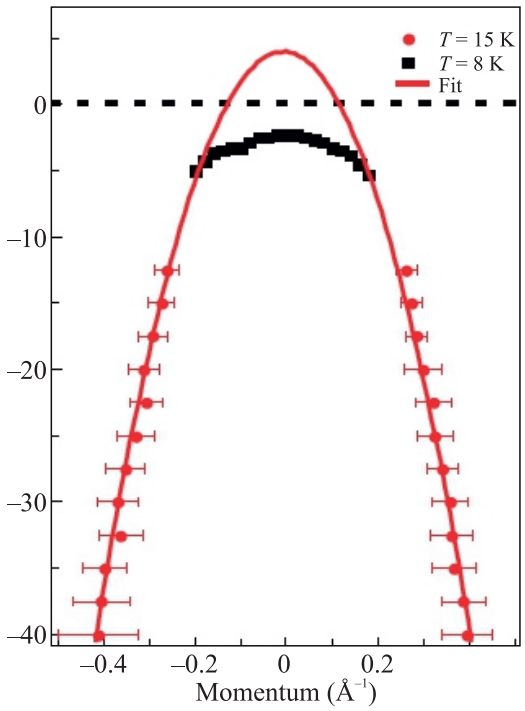

Fig. 10. (Color online) Dispersion of quasiparticles in the BCS–BEC crossover at temperatures above and below the critical temperature for $FeSe_xTe_{1-x}$. Adapted from [65].

ered at the Γ point, its value $\Delta = 2.3 \pm 0.3$ meV gives $\Delta/E_F \sim 0.5$, which indicates a strong interaction in $FeSe_xTe_{1-x}$ and the implementation of the BCS–BEC crossover (if the band were in the BEC state, the gap minimum would be located at k_F).

In [18], the superconductor $FeTe_{0.6}Se_{0.4}$ was investigated using laser spectroscopy with ultrahigh laser resolution. From the description of the experimental results it follows that this system also implements the mechanism discussed in Section 2. It was shown that superconductivity in this material occurs in the form of a coherent mixture of Cooper pairs forming in the hole band and a BCS–BEC crossover taking place in the electron band.

Figure 11 shows the spectrum of quasiparticles for temperatures below and above the critical one. Quantitative analysis of the spectra allows one to conclude that the electronic band is characterized by a small gap, but is in the strong coupling regime (BCS–BEC crossover). The hole band, on the contrary, has a larger gap and is in the relatively weak coupling regime (BCS). Panel (c) in Fig. 11 shows the combined band structure at temperatures above and below the critical one. It is noteworthy that the hole and electron bands merge in this band pattern, which is the evidence of the band interaction and electron-hole mixing regardless of the interaction strength.

Figure 11d shows the dependence of the superconducting gap for each of the bands as a function of temperature. The experiment clearly points to a pseudogap in the hole band, which quickly decreases when the gap appears in the electron band. However, in strong contradiction with the theory of the BCS–BEC crossover for single-band superconductors, a pseudogap could not be detected in the electronic band. This behavior of the pseudogap agrees with the fluctuation suppression mechanism discussed above.

4.3. Other Materials

In conclusion, we mention some other compounds in which the observation of BEC–BCS crossover, in our opinion, is promising for the implementation of the fluctuations suppression mechanism.

In [67], by changing the carrier density, a BCS–BEC crossover occurs in zirconium nitride chloride, an electron-doped two-dimensional superconductor. The phase diagram obtained by simultaneously measuring resistivity and ion-gated tunneling spectra demonstrates a pseudogap phase in the low-doping regime. The relationship between the superconducting transition temperature and the Fermi temperature in the low carrier density limit corresponds to the theoretical upper limit expected in the crossover regime. This system thus implements the two-dimensional BCS–BEC transition in a simple way.

In [68] the BCS–BEC crossover was implemented in an organic conductor with a triangular lattice $\kappa-(BEDT\text{-}TTF)_4Hg_{2.89}Br_8$. The parameter that controls the crossover in this case is external pressure which changes the Coulomb interaction between carriers.

In July 2023, the discovery of a new superconducting compound (LK-99) was reported with an extremely high transition temperature, apparently exceeding the room temperature [69, 70]. LK-99 is a copper-doped apatite, with the chemical formula $Pb_{10-x}Cu_x(PO_4)_6O$, $0.9 < x < 1.1$. The unit cell of this crystal structure is shown in Fig. 12. Attempts to reproduce the results reported in [69, 70] have produced mixed results but have generally been unsuccessful. Some experimental groups have confirmed the observation of the levitation [72], while others have reported its absence [73]. Some experiments confirm the conductivity jump, albeit at a different temperatures [74], while others find that the material is an insulator and exhibits paramagnetic behavior [75]. At the moment, the scientific community takes the room-temperature superconductivity in LK-99 with strong skepticism [76].

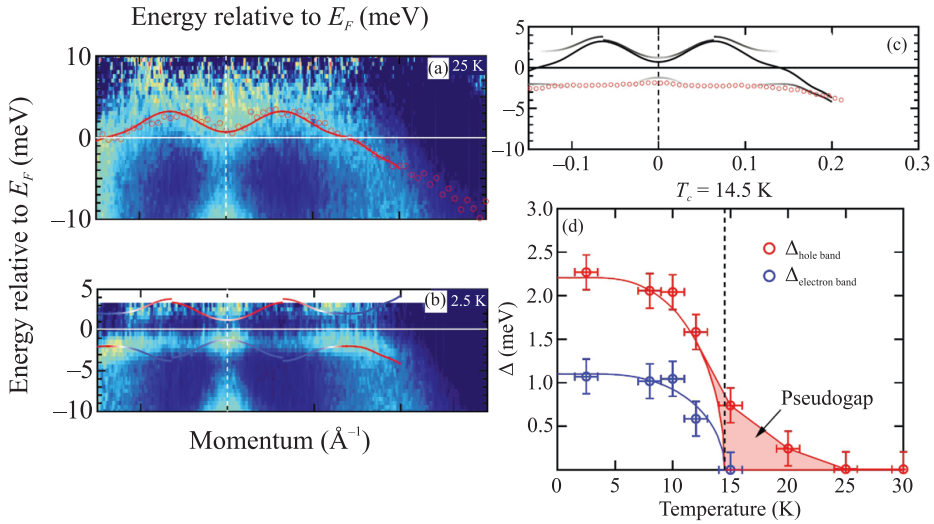

Fig. 11. (Color online) ARPES spectra for $FeTe_{0.6}Se_{0.4}$ above (a) and below (b) the critical temperature. The solid red curve in panel (a) is the result of fitting the dispersion curve marked with circles. The solid curves in panel (b) correspond to the dispersion of quasiparticles in the normal state, as well as for the superconducting gap $\Delta(k) = 2$ meV for the hole band and $\Delta(k) = 1$ meV for the electron band. (c) Dispersion curves from panels (a) and (b) on the same graph. (d) Temperature dependence of the superconducting gap for the electron and hole bands. The pseudogap region is shown in red. Adapted from [66].

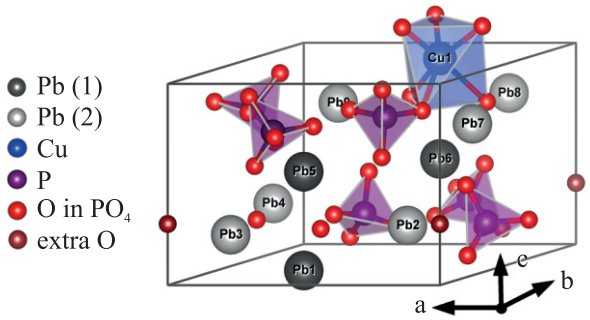

Fig. 12. (Color online) Crystal structure of LK-99. Copper atoms replacing lead form a triangular sublattice. Adapted from [71].

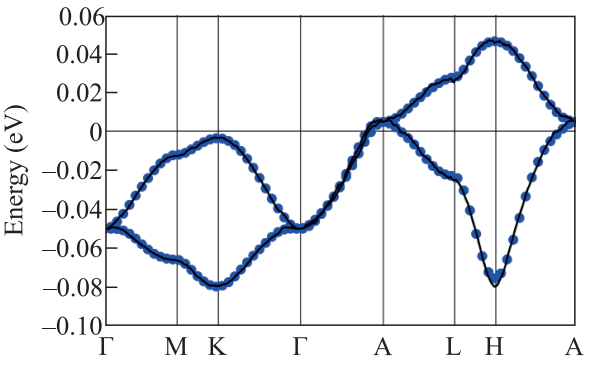

Fig. 13. (Color online) Band structure of LK-99 near the Fermi level. Adapted from [71].

Nevertheless, in view of the fluctuation suppression mechanism discussed above, LK-99, in our opinion, deserves close attention. Indeed, according to first-principle calculations of its band structure, two bands are active (close to the Fermi surface) in this material. One of these (see Fig. 13) is flat near its edge, and this results in a strong increase in the corresponding DOS. As a result, the mean-field critical temperature can be significantly enhanced, but only if the chemical potential is near the edge of the flat band. In this case, the inevitable temperature fluctuations in this shallow band are suppressed due to the interaction with another band. Note that the position of the chemical potential significantly depends on the presence of impurities and disorder, and in the case of a flat band with its almost singular nature of the DOS, a relatively small change in these factors can radically change the parameters of superconducting pairing and, accordingly, the temperature of the superconducting transition, possibly leading to a complete suppression of superconductivity.

5. CONCLUSIONS

In this review, we show that the coexistence of two interacting single-particle bands in a superconducting material, one of which is shallow and the other is not, can lead to the suppression of temperature fluctuations and stabilization of the BCS–BEC crossover regime in the shallow band. In the case that such a shallow band has a high density of single-particle states, for example, due to a van Hove singularity in a quasi-one-dimensional band, or due to a flat edge, the

fluctuation suppression mechanism can be expected to lead to a significant increase in the superconducting critical temperature. Due to the suppressed fluctuations, the latter will approach its value obtained in the mean field theory. An essential ingredient of this mechanism for suppressing fluctuations is that it becomes effective even at very low interband interactions, when the critical temperature is still determined by the shallow band.

The mechanism is not sensitive to the details of the band structure and can be found in a wide class of multiband materials. It is expected to occur in situations where more than two bands coexist in a material, as long as at least one of them is shallow and the interaction between them is not very strong.

Currently, there exist many materials in which this mechanism for stabilizing the BCS–BEC crossover and increasing the critical temperature can work. These include, in particular, materials with a quasi-one-dimensional structure and iron-based materials. An essential component of such materials is the presence of bands with a flat edge and the position of the Fermi level near it. It leads to a significant increase in the single particle DOS and, accordingly, the Cooper pairing. It is possible to achieve the desired position of the chemical potential in a material in various ways, for example, using chemical engineering, a change in the structure by applying external pressure or doping [60].

It should be noted that within the framework of the BCS theory, there is another mechanism for increasing the critical temperature that takes place due to broadening the energy window for the Cooper pairing, or the cutoff frequency ω_c. In this review, we do not consider this mechanism; we only note that it will act in parallel with the suppression of fluctuations due to the inter-band interactions in a multi-band structure.

FUNDING

The work was carried out within the framework of the "Priority 2030" program of the National Research Nuclear University MEPhI, and was also supported by the Ministry of Science and Higher Education of the Russian Federation (state task project no. FSWU-2023-0031). Arkady Shanenko and Alexei Vagov thank the Basic Research Program of the HSE Research University that was used to calculate the critical temperature shift. Vasily Stolyarov thanks for the support of the Russian Science Foundation (project no. 21-72-30026 https://rscf.ru/en/project/21-72-30026) and the Ministry of Science and Higher Education of the Russian Federation (state task project no. FSMG-2023-0014).

CONFLICT OF INTEREST

The authors of this work declare that they have no conflicts of interest.

REFERENCES

1. J. Bardeen, L. N. Cooper, and J. R. Schrieffer, Phys. Rev. B **108**, 1175 (1957).
2. J. G. Bednorz and K. A. Müller, Zeitschr. Phys., B **64**, 189 (1957).
3. V. J. Emery and S. A. Kivelson, Nature (London, U.K.) **374**, 434 (1995).
4. M. Buchanan, Nature (London, U.K.) **409**, 8 (2001).
5. M. V. Sadovskii, Phys. Usp. **44**, 515 (2001).
6. C. Varma, Nature (London, U.K.) **468**, 184 (2010).
7. S. I. Vedeneev, Phys. Usp. **64**, 890 (2021).
8. S. Borisenko, Nat. Mater. **12**, 600 (2013).
9. I. M. Lifshitz, Sov. Phys. JETP **38**, 1569 (1969).
10. G. E. Volovik, Low Temp. Phys. **43**, 47 (2017).
11. A. I. Coldea and M. D. Watson, Ann. Rev. Condens. Matter Phys. **9**, 125 (2018).
12. J. Ketterson and S. Song, *Superconductivity* (Cambridge Univ. Press, Cambridge, UK, 1999).
13. A. Larkin and A. Varlamov, *Theory of Fluctuations in Superconductors* (Oxford Univ. Press, Oxford, USA, 2005).
14. K. B. Efetov and A. I. Larkin, Sov. Phys. JETP **39**, 1129 (1974).
15. L. P. Gor'kov and I. E. Dzyaloshinskii, Sov. Phys. JETP **40**, 198 (1975).
16. D. Jérome, A. Mazaud, M. Ribault, and K. Bechgaard, J. Phys. Lett. **41**, 95 (1980).
17. Y. Lubashevsky, E. Lahoud, K. Chashka, D. Podolsky, and A. Kanigel, Nat. Phys. **8**, 309 (2012).
18. K. Okazaki, Y. Ito, Y. Ota, Y. Kotani, T. Shimojima, T. Kiss, S. Watanabe, C.-T. Chen, S. Niitaka, T. Hanaguri, H. Takagi, A. Chainani, and S. Shin, Sci. Rep. 4, (2014).
19. S. Kasahara, T. Watashige, Y. K. T. Hanaguri, T. Yamashita, Y. Shimoyama, Y. Mizukami, R. Endo, H. Ikeda, A. Kazushi, T. Terashima, S. Uji, T. Wolf, H. von Löhneysenf, T. Shibauchi, and Y. Matsuda, Proc. Natl. Acad. Sci. U. S. A. **111**, 16309 (2014).
20. S. Rinott, K. B. Chashka, A. Ribak, E. D. L. Rienks, A. Taleb-Ibrahimi, P. L. Fevre, F. Bertran, M. Randeria, and A. Kanigel, Sci. Adv. **3**, e1602372 (2017).
21. T. Hanaguri, S. Kasahara, J. Böker, I. Eremin, T. Shibauchi, and Y. Matsuda, Phys. Rev. Lett. **122**, 077001 (2019).
22. W. Huang, H. Lin, C. Zheng, Y. Yin, X. Chen, and S.-H. Ji, Phys. Rev. B **103**, 094502 (2021).
23. H. Lin, W. Huang, G. Rai, Y. Yin, L. He, Q.-K. Xue, S. Haas, S. Kettemann, X. Chen, and S.-H. Ji, Phys. Rev. B **107**, 104517 (2023).
24. Y. Mizukami, M. Haze, O. Tanaka, K. Matsuura, D. Sano, J. Böker, I. Eremin, S. Kasahara, Y. Matsuda, and T. Shibauchi, Commun. Phys. **6**, 183 (2023).

25. H. Suhl, B. T. Matthias, and L. R. Walker, Phys. Rev. Lett. **3**, 552 (1959).

26. V. A. Moskalenko, Phys. Met. Metallogr. **8**, 25 (1959).

27. M. Greiner, C. A. Regal, and D. S. Jin, Nature (London, U.K.) **426**, 537 (2003).

28. I. Bloch, J. Dalibard, and W. Zwerger, Rev. Mod. Phys. **80**, 885 (2008).

29. L. P. Gor'kov, Sov. Phys. JETP **9**, 1364 (1959).

30. H. Doh, M. Sigrist, B. K. Cho, and S.-I. Lee, Phys. Rev. Lett. **83**, 5350 (1999).

31. I. Askerzade, A. Gencer, and N. Güçlü, Supercond. Sci. Technol. **15**, L13 (2002).

32. I. Askerzade, A. Gencer, and N. Güçlü, Supercond. Sci. Technol. **15**, L17 (2002).

33. T. T. Saraiva, P. J. F. Cavalcanti, A. Vagov, A. S. Vasenko, A. Perali, L. Dell'Anna, and A. A. Shanenko, Phys. Rev. Lett. **125**, 217003 (2020).

34. A. A. Shanenko, T. T. Saraiva, A. Vagov, A. S. Vasenko, and A. Perali, Phys. Rev. B **105**, 214527 (2022).

35. V. L. Ginzburg and L. D. Landau, Zh. Eksp. Teor. Fiz. **20**, 1064 (1950).

36. L. Salasnich, A. A. Shanenko, A. Vagov, J. A. Aguiar, and A. Perali, Phys. Rev. B **100**, 064510 (2019).

37. T. T. Saraiva, L. I. Baturina, and A. A. Shanenko, J. Phys. Chem. Lett. **12**, 11604 (2021).

38. B. T. Geilikman, R. O. Zaitsev, and V. Z. Kresin, Sov. Phys. Solid State **9**, 642 (1967).

39. V. Z. Kresin, J. Low Temp. Phys. **11**, 519 (1973).

40. J. Geyer, R. M. Fernandes, V. G. Kogan, and J. Schmalian, Phys. Rev. B **82**, 104521 (2010).

41. A. A. Shanenko, M. V. Miloševic, F. M. Peeters, and A. V. Vagov, Phys. Rev. Lett. **106**, 047005 (2011).

42. A. Z. Pokrovskii and V. L. Patashinskii, *Fluctuation Theory of Phase Transitions* (Pergamon, Oxford, USA, 1999).

43. D. R. Nelson and J. M. Kosterlitz, Phys. Rev. Lett. **39**, 1201 (1977.

44. A. L. Fetter and J. D. Walecka, *Quantum Theory of Many-Particle Systems* (Dover, New York, 2003).

45. A. Vagov, A. A. Shanenko, M. V. Miloševic, V. M. Axt, V. M. Vinokur, J. A. Aguiar, and F. M. Peeters, Phys. Rev. B **93**, 174503 (2016).

46. S. Wolf, A. Vagov, A. A. Shanenko, V. M. Axt, A. Perali, and J. A. Aguiar, Phys. Rev. B **95**, 094521 (2017).

47. J. M. Kosterlitz and D. J. Thouless, J. Phys. C: Solid State Phys. **6**, 1181 (1973).

48. P. G. de Gennes, *Superconductivity of Metals and Alloys* (CRC, New York, 1999).

49. A. Vagov, A. A. Shanenko, M. V. Miloševic, V. M. Axt, and F. M. Peeters, Phys. Rev. B **86**, 144514 (2012).

50. A. Cappellaro and L. Salasnich, Sci. Rep. **10**, 9088 (2020).

51. H. Z. Zhi, T. Imai, F. L. Ning, J.-K. Bao, and G.-H. Cao, arXiv: 1501.00713 (2015).

52. C. C. Hao Jiang and Guanghan Cao, arXiv: 1412.1309 (2015).

53. R. Brusetti, P. Monceau, M. Potel, P. Gougeon, and M. Sergent, Solid State Commun. **66**, 181 (1988).

54. J.-F. Mercure, A. F. Bangura, X. Xu, N. Wakeham, A. Carrington, P. Walmsley, M. Greenblatt, and N. E. Hussey, Phys. Rev. Lett. **108**, 187003 (2012).

55. J.-K. Bao, J.-Y. Liu, C.-W. Ma, Z.-H. Meng, Z.-T. Tang, Y.-L. Sun, H.-F. Zhai, H. Jiang, H. Bai, C.-M. Feng, Z.-A. Xu, and G.-H. Cao, Phys. Rev. X **5**, 011013 (2015).

56. Z.-T. Tang, J.-K. Bao, Y. Liu, Y.-L. Sun, A. Ablimit, H.-F. Zhai, H. Jiang, C.-M. Feng, Z.-A. Xu, and G.-H. Cao, Phys. Rev. B **91**, 020506(R) (2015).

57. Z.-T. Tang, J.-K. Bao, Z. Wang, H. Bai, H. Jiang, Y. Liu, H.-F. Zhai, C.-M. Feng, Z.-A. Xu, and G.-H. Cao, Sci. China Mater. **58**, 16 (2015).

58. C. Xu, N. Wu, G.-X. Zhi, B.-H. Lei, X. Duan, F. Ning, C. Cao, and Q. Chen, npj Comput. Mater. **6**, 30 (2020).

59. H. Lin, W. Huang, G. Rai, Y. Yin, L. He, Q.-K. Xue, S. Haas, S. Kettemann, X. Chen, and S.-H. Ji, arXiv: 2209.00758 (2023).

60. S.-Q. Wu, C. Cao, and G.-H. Cao, Phys. Rev. B **100**, 155108 (2019).

61. J. Ranninger and J. M. Robin, Phys. Rev. B **53**, R11961 (1996).

62. J. Sous, Y. He, and S. A. Kivelson, npj Quantum Mater. **8**, 25 (2023).

63. T. Terashima, N. Kikugawa, A. Kiswandhi, et al., Phys. Rev. B **90**, 144517 (2014).

64. . Q. Chen, J. Stajic, S. Tan, and K. Levin, Phys. Rep. **412**, 1 (2005).

65. Y. Lubashevsky, E. Lahoud, K. Chashka, D. Podolsky, and A. Kanigel, arXiv: 1107.1487 (2012).

66. K. Okazaki, Y. Ito, Y. Ota, Y. Kotani, T. Shimojima, T. Kiss, S. Watanabe, C.-T. Chen, S. Niitaka, T. Hanaguri, H. Takagi, A. Chainani, and S. Shin, arXiv: 1307.7845 (2014).

67. Y. Nakagawa, Y. Kasahara, T. Nomoto, R. Arita, T. Nojima, and Y. Iwasa, Science (Washington, DC, U. S.) **372**, 190 (2021).

68. Y. Suzuki, K. Wakamatsu, J. Ibuka, H. Oike, T. Fujii, K. Miyagawa, H. Taniguchi, and K. Kanoda, Phys. Rev. X **12**, 011016 (2022).

69. S. Lee, J.-H. Kim, and Y.-W. Kwon, arXiv: 2307.12008 (2023).

70. S. Lee, J. Kim, H.-T. Kim, S. Im, S. An, and K. H. Auh, arXiv: 2307.12037 (2023).

71. L. Si, M. Wallerberger, A. Smolyanyuk, S. di Cataldo, J. M. Tomczak, and K. Held, arXiv: 2308.04427 (2023).

72. H. Wu, L. Yang, B. Xiao, and H. Chang, arXiv: 2308.01516 (2023).

73. K. Kumar, N. K. Karn, Y. Kumar, and V. P. S. Awana, arXiv: 2308.03544 (2023).

74. Q. Hou, W. Wei, X. Zhou, Y. Sun, and Z. Shi, arXiv: 2308.01192.

75. Y. Jiang, S. B. Lee, J. Herzog-Arbeitman, J. Yu, X. Feng, H. Hu, D. Calugaru, P. S. Brodale, E. L. Gormley, M. G. Vergniory, C. Felser, S. Blanco-Canosa, C. H. Hendon, L. M. Schoop, and B. A. Bernevig, arXiv: 2308.05143 (2023).

76. D. Garisto, Nature (London, U.K.) **620**, 705 (2023).

SPELL: OK